DETECTION OF CHIPPING IN CERAMIC CUTTING INSERTS FROM WORKPIECE PROFILE SIGNATURE DURING TURNING PROCESS USING MACHINE VISION

LEE WOON KIOW

UNIVERSITI SAINS MALAYSIA

2017

DETECTION OF CHIPPING IN CERAMIC CUTTING INSERTS FROM WORKPIECE PROFILE SIGNATURE DURING TURNING PROCESS USING MACHINE VISION

by

LEE WOON KIOW

Thesis submitted in fulfillment of the requirements for the degree of Doctor of Philosophy

May 2017

ACKNOWLEDGEMENTS

First and foremost, I would like to express my sincere gratitude to my supervisor Professor Dr. Mani Maran Ratnam for his supervision, advice and support since the first beginning of my research. His guidance helped me in all the time of the research and writing of this thesis. Special thanks are also given to my co-supervisor Professor Dr. Zainal Arifin Bin Ahmad for his help and encouragement in my research.

My sincere thanks also goes to the laboratory staffs who have helped me a lot in the laboratory and experimental work. They are Mr. Mohd Shawal Faizal Ismail (Machining laboratory), Mr. Mohd Ashamuddin Hashim (Microscopy and micro analysis laboratory) and Mr. Wan Mohd Amri Bin Wan Mamat Ali (Vibration laboratory) for their support and valuable time to complete this research.

Last but not the least, I would like to thank my parents and family members for their continuous encouragement, support, unlimited dedication and love throughout so many years. My sincere appreciation also extends to all my colleagues and friends who supported me spiritually throughout the entire PhD study.

TABLES OF CONTENTS

	Page
ACKNOWLEDGEMENT	**ii**
TABLE OF CONTENTS	**iii**
LIST OF TABLES	**vii**
LIST OF FIGURES	**viii**
LIST OF ABBREVIATIONS	**xvi**
LIST OF SYMBOLS	**xviii**
ABSTRAK	**xxi**
ABSTRACT	**xxiii**
CHAPTER ONE: INTRODUCTION	
1.1 Background of study	1
1.2 Problem statement	7
1.3 Objectives	8
1.4 Research approach	9
1.5 Scope of study	9
1.6 Organization of thesis	9
CHAPTER TWO: LITERATURE REVIEW	
2.1 Introduction	11
2.2 Types of tool failure	11
2.3 Monitoring of gradual wear	14
2.3.1 Monitoring of gradual wear using direct method	14
2.3.2 Monitoring of gradual wear using indirect method	18
2.4 Detection of tool failure by chipping	25

2.5 Detection of tool failure in ceramic cutting tool 29

2.6 Detection of tool failure from the workpiece surface using machine vision and image processing method 31

2.7 Signal processing method 34

2.7.1 Time domain analysis 35

2.7.2 Frequency domain analysis 37

2.7.3 Time-frequency domain analysis 38

2.8 Chapter summary 40

CHAPTER THREE: METHODOLOGY

3.1 Introduction 43

3.2 In-process tool chipping detection in ceramic cutting insert from the workpiece profile signature using ACF 45

3.2.1 Simulation work 45

3.2.2 Experimental work 60

3.2.3 Machining condition 61

3.2.4 Image acquisition system 61

3.2.5 Scaling factor determination 65

3.2.6 Distortion assessment 67

3.2.7 Description of workpiece profile detection algorithm in sub-pixel level accuracy edge detection using invariant moment method 68

3.2.8 Motion blurring effect assessment 75

3.3 Detection of tool chipping in ceramic cutting insert from the workpiece profile signature using FFT 76

3.3.1 Simulation work on detection of tool chipping from surface profile signature using FFT by considering the geometry changes of tool nose 77

3.3.2 Offline experimental work 86

3.3.3 Simulation work on detection of tool chipping from surface profile signature using FFT by considering the presence of tool-workpiece vibration 87

3.3.4 In-process experimental work 88

3.3.5 In-process detection of tool chipping from surface profile signature using sub-window FFT 91

3.4 In-process detection of tool chipping from workpiece profile signature using CWT 92

3.5 Chapter summary 97

CHAPTER FOUR: RESULTS AND DISCUSSIONS

4.1 Introduction 99

4.2 In-process detection of chipping in ceramic cutting insert based on the surface profile signature using ACF 100

4.2.1 Simulation results 100

4.2.2 Experimental results 103

4.3 Detection of tool chipping in ceramic cutting insert from the surface profile signature using FFT 119

4.3.1 Simulation results on detection of tool chipping from surface profile signature using FFT by considering the changes of the tool nose 119

4.3.2 Results of offline experiment 123

4.3.3 Simulation results on detection of tool chipping from surface profile signature using FFT by considering the presence of tool-workpiece vibration 133

4.3.4 Results of in-process experiment 135

4.3.5 Results of in-process onset detection of tool chipping from surface profile signature using sub-window FFT 143

4.4 Results of in-process onset detection of chipping in ceramic cutting insert based on the surface profile signature using CWT 152

4.4.1 Results of repeat experiment 159

4.5 Chapter summary 161

CHAPTER FIVE: CONCLUSION AND RECOMMENDATIONS

5.1	Introduction	163
5.2	Conclusions	163
5.3	Contributions of study	165
5.4	Future recommendations	165

REFERENCES 167

APPENDICES

Appendix A [Repeated experimental results of FFT]

Appendix B [Repeated experimental results of sub-window FFT]

Appendix C [Repeated experimental results of CWT]

LIST OF PUBLICATIONS

LIST OF TABLES

		Page
Table 2.1	Summary of the methods and their limitations	41
Table 3.1	Number of pixels between measurement points	68
Table 3.2	Validation of the roughness values (R_a, R_q and R_t) obtained from vision method by comparing the roughness values(R_a, R_q and R_t) obtained from stylus method	74
Table 3.3	Number of pixels between the wavelength	76
Table 4.1	Average of spectrum amplitude at spatial frequencies lower than the fundamental feed frequency.	151

LIST OF FIGURES

		Page
Figure 2.1	(a) Tool-workpiece interaction, and (b) location of crater wear and flank wear (Özel and Davim, 2009)	12
Figure 2.2	Typical flank wear versus time curve (Wang and Gao, 2006)	12
Figure 2.3	Typical wear pattern according to ISO 3685 (1993)	13
Figure 2.4	Tool failure by chipping and breakage (Grzesik, 2008a)	14
Figure 2.5	The framework of tool condition monitoring using indirect method (Lauro et al., 2014)	34
Figure 3.1	Flow of research methodology	44
Figure 3.2	The flow chart of the generation of ideal workpiece profile	46
Figure 3.3	Geometry of the nose profile created using *AUTOCAD*	47
Figure 3.4	Schematic representation of interaction between the cutting tool tip and the formed surface	48
Figure 3.5	Simulated ideal workpiece profile generated from *AUTOCAD*	48
Figure 3.6	Simulated ideal workpiece profile extracted from Figure 3.5 using vertical orthogonal scanning	50
Figure 3.7	(a) Simulated surface profile with increasing vibration amplitudes by 5% peak-to-valley height of simulated ideal workpiece profile; (b) simulated surface profile with increasing vibration amplitudes by 10% peak-to-valley height of simulated ideal workpiece profile; (c) simulated surface profile with random vibration with 5 times higher vibration magnitude as in (a); (d) simulated surface profile with random vibration with 10 times higher vibration magnitude as in (a); and (e) simulated surface profile with presence of waviness due to the tool-workpiece vibration by 10 times higher vibration magnitude as in (a)	54
Figure 3.8	Flow chart for ACF algorithm	58
Figure 3.9	Mechanism of ACF	59
Figure 3.10	Experiment setup for in-process image acquisition during turning operation	62

Figure 3.11	Close-up side view of the image acquisition configuration	63
Figure 3.12	Image of the edge of the workpiece captured by DSLR camera	63
Figure 3.13	Workpiece rotation angle determination	64
Figure 3.14	(a) Image of pin gage captured vertically, and (b) binarization of cropped ROI to determine the scaling factor	66
Figure 3.15	Images of Ronchi ruling (a) vertical, and (b) horizontal	67
Figure 3.16	Flow chart of algorithm for surface profile detection	69
Figure 3.17	Invariant moment method	71
Figure 3.18	Workpiece profile extraction (a) orthogonal scanning, and (b) workpiece profile with sub-pixel edge location	73
Figure 3.19	Surface profile obtained from (a) vision method, and (b) stylus method	74
Figure 3.20	Motion blurring assessment by comparing the number of pixels between the wavelength of workpiece profile	75
Figure 3.21	(a) Schematic representation of interaction between the cutting tool tip and the formed surface, and (b) formation of tool wear by increasing the radius in minor axis	77
Figure 3.22	Simulated cutting tool (a) unworn, (b) gradual wear by increase 1% of r_ε in the minor axis, (c) gradual wear by increase 2% of r_ε in the minor axis, (d) gradual wear by increase 3% of r_ε in the minor axis, (e) gradual wear by increase 4% of r_ε in the minor axis, (f) gradual wear by increase 5% of r_ε in the minor axis, (g) gradual wear by increase 6% of r_ε in the minor axis, and (h) gradual wear by increase 7% of r_ε in the minor axis	78
Figure 3.23	Simulated workpiece profile corresponding to the simulated worn tool in Figure 3.22	79
Figure 3.24	Tool nose area showing the maximum peak-to-valley height R_t of workpiece profile generated from worn and unworn tool profile	80
Figure 3.25	Formation of chipping by removing a cavity from tool nose region	81
Figure 3.26	Simulated worn tool for chipping	81

Figure 3.27	Simulated workpiece profile corresponding to the simulated chipped tool in Figure 3.26	82
Figure 3.28	Simulated worn tool from evolution of gradual wear to chipped tool	83
Figure 3.29	Simulated workpiece profile corresponding to the simulated worn tool in Figure 3.28	83
Figure 3.30	Offline image acquisition configuration	87
Figure 3.31	In-process experiment setup with vibration measurement	89
Figure 3.32	Flow chart for FFT analysis of actual workpiece profile for offline and in-process tool chipping detection in ceramic cutting tool	90
Figure 3.33	Flow chart for CWT algorithm	93
Figure 3.34	(a) Morlet wavelet, and (b) wavelet analysis overview	95
Figure 3.35	Wavelet analysis to produce scalogram	96
Figure 4.1	(a)(i) Ideal workpiece profile and (ii)corresponding peak of ACF plot; (b)(i) simulated surface profile with increasing vibration amplitudes by 5% peak-to-valley height of simulated ideal workpiece profile and (ii) corresponding peak of ACF plot; (c)(i) simulated surface profile with increasing vibration amplitudes by 10% peak-to-valley height of simulated ideal workpiece profile and (ii) corresponding peak of ACF plot (ii); (d)(i) simulated surface profile with random vibration with 5 times higher magnitude as in (b) and (ii) corresponding peak of ACF plot; (e)(i) simulated surface profile with random vibration with 10 times higher magnitude as in (b) and (ii) corresponding peak of ACF plot; and (f) simulated surface profile with presence of waviness due to the tool-workpiece vibration by 10 times higher vibration magnitude as in (b) and (ii) corresponding peak of ACF plot	101
Figure 4.2	ACF plot of workpiece profile generated by aluminium oxide ceramic cutting insert at different rotational angles within cutting time interval of (a) 0-5.5 s, (b) 5.6-11.0 s, (c) 11.1-16.5 s, (d) 16.6-22.0 s, (e) 22.1-27.5 s, and (f) 27.6-33.0 s	104
Figure 4.3	SEM micrographs of aluminium oxide ceramic cutting insert after machining (a) before chipping, and (b) after chipping	105

Figure 4.4	3-D observation of the chipping on the cutting edge by *Alicona Infinite Focus*	105
Figure 4.5	Extracted surface roughness profile from 2-D workpiece images at different rotational angles (a) 0^o, (b) 60^o, (c) 120^o, (d) 180^o, (e) 240^o, and (f) 300^o in cutting time interval of 0-5.5 s	106
Figure 4.6	Extracted surface roughness profile from 2-D workpiece images at different rotational angles (a) 0^o, (b) 60^o, (c) 120^o, (d) 180^o, (e) 240^o, and (f) 300^o in cutting time interval of 5.6-11.0 s	107
Figure 4.7	Zoomed view of 2-D images of the workpiece profile and the corresponding extracted surface roughness profile before tool chipping	108
Figure 4.8	Extracted surface roughness profile from 2-D workpiece images at different rotational angles (a) 0^o, (b) 60^o, (c) 120^o, (d) 180^o, (e) 240^o, and (f) 300^o in cutting time interval of 11.1-16.5 s	110
Figure 4.9	Extracted surface roughness profile from 2-D workpiece images at different rotational angles (a) 0^o, (b) 60^o, (c) 120^o, (d) 180^o, (e) 240^o, and (f) 300^o in cutting time interval of 16.6-22.0 s	111
Figure 4.10	Extracted surface roughness profile from 2-D workpiece images at different rotational angles (a) 0^o, (b) 60^o, (c) 120^o, (d) 180^o, (e) 240^o, and (f) 300^o in cutting time interval of 22.1-27.5 s	112
Figure 4.11	Extracted surface roughness profile from 2-D workpiece images at different rotational angles (a) 0^o, (b) 60^o, (c) 120^o, (d) 180^o, (e) 240^o, and (f) 300^o in cutting time interval of 27.6-33.0 s	113
Figure 4.12	Zoomed view of 2-D images of the workpiece profile and the corresponding extracted surface roughness profile after tool chipping	114
Figure 4.13	Peak of ACF of the simulated ideal workpiece profile against with the lag distance	116
Figure 4.14	3-D bar plot of SSD from the autocorrelation peak for the ideal workpiece profile: (a) front view, and (b) back view	117

Figure 4.15	ACF plot of workpiece profile generated by aluminium oxide ceramic cutting insert at different rotational angles for repeat experiment (a) before tool chipping, and (b) after tool chipping	118
Figure 4.16	(a) Simulated ideal workpiece profile, and (b) FFT analysis for simulated ideal workpiece profile	120
Figure 4.17	Variation of the amplitude of fundamental feed frequency, second harmonic and third harmonic of the simulated surface profile for gradual wear	121
Figure 4.18	Variation of the amplitude of fundamental feed frequency, second harmonic and third harmonic of simulated surface profile for chipping	122
Figure 4.19	Variation of the amplitude of fundamental feed frequency of the simulated surface profile from gradual wear to chipping	122
Figure 4.20	Tool nose area showing the maximum peak-to-valley height R_t of workpiece profile generated from unworn and chipped tool profile	123
Figure 4.21	SEM observation of carbide cutting insert before and after machining (a) isometric view, and (b) top view	124
Figure 4.22	Variation of the amplitude of fundamental feed frequency, second harmonic and third harmonic of actual surface profile from turning stainless steel work piece using carbide insert in (a) cutting time duration of 76.3 s, and (b) cutting time duration of 8 minutes	125
Figure 4.23	Example of FFT analysis for actual surface profile obtained from experiment using carbide cutting insert	126
Figure 4.24	2-D images of the workpiece profile from turning with carbide cutting insert and their corresponding surface roughness profile at cutting time duration of (a) 8.5 s, (b) 50.9 s, and (c) 84.8 s	127
Figure 4.25	Peak-to-valley roughness parameter (R_t) as a function of cutting time for carbide insert	128
Figure 4.26	SEM observation of the ceramic cutting insert before and after machining (a) isometric view, and (b) top view	129
Figure 4.27	Variation of the amplitude of fundamental feed frequency, second harmonic and third harmonic of actual surface profile from turning stainless steel workpiece using ceramic insert.	130

Figure 4.28 2-D images of the edge of workpiece from turning with ceramic cutting insert and their corresponding surface roughness profile at cutting time duration of (a) 8.5 s, (b) 50.9 s, and (c) 84.8 s 131

Figure 4.29 Peak-to-valley roughness parameter (R_t) as a function of cutting time for ceramic insert 132

Figure 4.30 (a)(i) Simulated surface profile with increasing vibration amplitudes by 5% peak-to-valley height of simulated ideal workpiece profile and (ii) corresponding FFT plot; (b)(i) simulated surface profile with increasing vibration amplitudes by 10% peak-to-valley height of simulated ideal workpiece profile and (ii) corresponding FFT plot (ii); (c)(i) simulated surface profile with random vibration with 5 times higher vibration magnitude as in (a) and (ii) corresponding FFT plot; (d)(i) simulated surface profile with random vibration with 10 times higher vibration magnitude as in (a) and (ii) corresponding FFT plot; and (e) simulated surface profile with presence of waviness due to the tool-workpiece vibration by 10 times higher vibration magnitude as in (a) and (ii) corresponding FFT plot 134

Figure 4.31 Zoomed in actual workpiece profile at different rotation angles (a) 0^o, (b) 60^o, (c) 120^o, (d) 180^o, (e) 240^o, (f) 300^o and their corresponding extracted sub-pixel profile at cutting duration of 5.5 s 137

Figure 4.32 Zoomed in actual workpiece profile at different rotation angles (a) 0^o, (b) 60^o, (c) 120^o, (d) 180^o, (e) 240^o, (f) 300^o and their corresponding extracted sub-pixel profile at cutting duration of 5.6-11.0 s 138

Figure 4.33 Zoomed in actual workpiece profile at different rotation angles (a) 0^o, (b) 60^o, (c) 120^o, (d) 180^o, (e) 240^o, (f) 300^o and their corresponding extracted sub-pixel profile at cutting duration of 11.1-16.5 s 139

Figure 4.34 Zoomed in actual workpiece profile at different rotation angles (a) 0^o, (b) 60^o, (c) 120^o, (d) 180^o, (e) 240^o, (f) 300^o and their corresponding extracted sub-pixel profile at cutting duration of 16.6-22.0 s 140

Figure 4.35 FFT of the actual workpiece profile for each pass and their corresponding cutting tool condition at cutting time duration of (a) 5.5 s, (b) 11.0 s, (c) 16.5 s, and (d) 22.0 s 141

Figure 4.36 Examples of zoomed in FFT plot (a) before, and (b) after tool chipping 142

Figure 4.37	Variation in the amplitude of the fundamental feed frequency of the workpiece profile with cutting duration at various workpiece rotation angles	142
Figure 4.38	Sub-window of the FFT along the workpiece profile at different rotational angles (a) 0^o, (b) 120^o, and (c) 240^o in cutting time duration of 0-5.5 s	144
Figure 4.39	Sub-window of the FFT along the workpiece profile at different rotational angles (a) 0^o, (b) 120^o, and (c) 240^o in cutting time duration of 5.6-11.0 s	145
Figure 4.40	Sub-window of the FFT along the workpiece profile at different rotational angles (a) 0^o, (b) 120^o, and (c) 240^o in cutting time duration of 11.1-16.5 s	146
Figure 4.41	Sub-window of the FFT along the workpiece profile at different rotational angles (a) 0^o, (b) 120^o, and (c) 240^o in cutting time duration of 16.5-22.0 s	147
Figure 4.42	Vibration measurement within cutting time duration of (a) 5.5 s, (b) 11.0 s, (c) 16.5 s, and (d) 22.0 s	149
Figure 4.43	Zoomed sub-window of FFT of the workpiece profile for (a) before tool chipping, and (b) after tool chipping	150
Figure 4.44	Standard deviation of the amplitude of FFT for each sub-window at various rotational workpiece angle	152
Figure 4.45	(a) simulated workpiece profile, and (b) scalogram for simulated ideal workpiece profile	153
Figure 4.46	Scalograms corresponding to the workpiece profile in Figure 4.38(a)(ii)-(c)(ii)	154
Figure 4.47	Scalograms corresponding to the workpiece profile in Figure 4.39(a)(ii)-(c)(ii)	154
Figure 4.48	Scalograms corresponding to the workpiece profile in Figure 4.40(a)(ii)-(c)(ii)	155
Figure 4.49	Scalograms corresponding to the workpiece profile in Figure 4.41(a)(ii)-(c)(ii)	156
Figure 4.50	RMS of CWT coefficient at different scales (a) 20, (b) 60, (c) 100, and (d) comparison of maximum deviation of RMS of CWT coefficients	157

Figure 4.51	Comparison of the sub-window FFT and CWT in onset tool chipping detection (a) sub-window FFT analysis, (b) workpiece profile, and (c) CWT analysis	158
Figure 4.52	Examples of zoomed-in FFT plot (a) before, and (b) after tool chipping at workpiece rotation angle of 120^o for repeat experiment	159
Figure 4.53	Sub-window of the FFT along the workpiece (a) before, and (b) after tool chipping at workpiece rotation angle of 120^o for repeat experiment	160
Figure 4.54	Scalograms corresponding to the workpiece profile in Figure 4.53(a)(ii) and Figure 4.53(b)(ii)	160
Figure 4.55	Comparison of maximum deviation of RMS of CWT coefficients (a) before, and (b) after tool chipping at scales of 20, 60 and 100 for various workpiece rotation angles	161

LIST OF ABBREVIATIONS

2-D	Two dimensional
3-D	Three dimensional
ACF	Autocorrelation function
AE	Acoustic emission
AFM	Atomic force microscopes
AISI	American Iron and Steel Institute
ASME	American Society of Mechanical Engineers
CCD	Charge coupled device
CPU	Central processing unit
CWT	Continuous wavelet transform
DFT	Discrete Fourier transform
DSLR	Digital single-lens-reflex
DWT	Discrete wavelet transform
FFT	Fast Fourier transform
GLCM	Gray level co-occurrence matrix
ISO	International Organization for Standardization
MVIM	Multi-valued influence matrix
PCBN	Polycrystalline cubic boron nitride
PSD	Power spectral density
RGB	Red Green Blue
RMS	Root mean square
ROI	Region of interest
SEM	Scanning electron microscope

SSA	Singular spectrum analysis
SSD	Sum square of deviation
STFT	Short time Fourier transform
SVM	Support vector machine
TSK	Takagi-Sugeno-Kang

LIST OF SYMBOLS

$*$	Complex conjugation
ϕ	Random dislocation of the workpiece profile caused by chipping
λ	wavelength of the surface waviness
π	Pi
τ	Lag distance
$\Delta\tau$	Lag interval
β	Workpiece rotation angle between successive images
α	Sample variance
γ	Average of amplitude spectrum in a specific spatial frequency band
$\psi(t)$	Mother wavelet
$\psi_{b,a}(t)$	Wavelet basis/ wavelet function
a	Dilation/ scale
a_n	Coefficients of the cosine term
$A(\tau)$	Autocorrelation function coefficient
$A(m\Delta\tau)$	Autocorrelation function coefficient for discrete data
b	Translation
b_n	Coefficients of the sine term
C_n	Amplitude of dislocation in the workpiece profile
$CWT(a,b)$	Wavelet coefficient
d_1, d_2, d_3	Number of pixels between the wavelength
exp	Exponential
f	Feed /feed rate
F_1, F_2	frequency range

$G(x)$	Actual surface profile/ unshifted surface profile
$G(x+\tau)$	Shifted surface profile
$G(i)$	Surface profile at position $m\Delta\tau$
$G(i-m)$	Surface profile at position $(i-m)\Delta\tau$
$G(t)$	Surface profile in time domain
h_1, h_2	Brightness
I_p	Intersection points between the nose profile and workpiece
i	Column in image of workpiece profile
j	Complex number
K	Sub-pixel edge location of the workpiece
L	Total length of workpiece profile
m	Integer number
$\overline{m}_i$	Moments of the input data sequence in the gray-scale image
n	Number of input data
n_R	Number of rotations
N	Total number of pixel/ points in the workpiece profile
O	Centre of the nose profile
p_1, p_2	densities of the gray level brightness
r_ε	Nose radius
R_a	Arithmetic average height of surface profile
R_t	Peak-to-valley height of the surface profile
R_p	Maximum height of peaks
R_q	Root mean square roughness
R_q^2	Square of root mean square roughness
$RMSW_a$	RMS of CWT coefficient at particular scale of *a*

s	Skewness
S	capturing time between the successive images
t	Time
$u(x)$	Dislocation profile results from the vibration
$U_{gs}(x)$	Ideal surface profile
V	Spindle rotational speed
V_f	Fundamental feed frequency
V_n	Spatial frequencies
VB	Width of wear land
VB_B	Average flank wear
VB_{max}	Maximum flank wear
w	Length of window
ω	Fundamental angular frequency
x	x vector for x-coordinate of surface profile
x_n	Length of workpiece profile at particular position
x_z	Intensity of the pixel in gray-scale images
(x_i, y_i)	Coordinate of surface profile
y	y vector for y-coordinate of surface profile
$Y(\omega)$	Amplitude of spatial frequencies for continuous Fourier transform
$Y(V_n)$	Amplitude of spatial frequencies for discrete Fourier transform
z	Row in image

PENGESANAN SERPIHAN PADA MATA ALAT SERAMIK DARIPADA TANDA PENGENALAN PROFIL BAHAN KERJA SEMASA PROSES PELARIKAN MENGGUNAKAN PENGLIHATAN MESIN

ABSTRAK

Mata alat seramik lebih cenderung kepada kegagalan menjadi serpihan bukannya kehausan berterusan disebabkan oleh keliatan hentamannya yang rendah. Mata alat menjadi serpihan akan menyebabkan kualiti permukaan dan ketepatan dimensi merosot. Oleh itu, pengesanan dalam proses kegagalan tersebut pada mata alat seramik amat penting terutamanya dalam pengendalian pemesinan tidak berjaga. Kaedah pengesanan kegagalan mata alat dalam proses dengan menggunakan isyarat penderia yang wujud mempunyai had keupayaannya untuk mengesan serpihan mata alat. Pengawasan malat alat daripada profil bahan kerja dengan menggunakan penglihatan mesin mempunyai potensi yang tinggi digunakan semasa proses pemesinan, tetapi tiada percubaan dibuat untuk mengesan kegagalan serpihan mata alat. Dalam kerja ini, kaedah penglihatan mesin dibangunkan untuk mengesan kegagalan serpihan mata alat seramik daripada tanda pengenalan profil 2-D bahan kerja. Profil permukaan bahan kerja bertentangan dengan mata alat dirakam semasa pelarikan dengan menggunakan kamera DSLR. Profil permukaan bahan kerja diekstrak kepada ketepatan sub-piksel dengan menggunakan kaedah momen ketakvarianan. Kesan serpihan mata alat seramik pada tanda pengenalan profil permukaan bahan kerja disiasat dengan menggunakan fungsi autokorelasi (ACF) dan transformasi Fourier cepat (FFT). Pengesanan kegagalan serpihan dijalankan dengan sub-tetingkap FFT dan transformasi gelombang selanjar (CWT). Kegaglan serpihan mata alat seramik menyebabkan puncak ACF profil bahan kerja merosot cepat apabila jarak susul meningkat dan melencong dengan nyata pada sudut putaran bahan kerja yang berlainan. Amplitud frekuensi suapan asas semakin meningkat dengan masa apabila kehausan mata alat berlaku. Akan tetapi amplitud frekuensi suapan

turun naik dengan nyata selepas mata alat gagal menjadi serpihan. Proses pemotongan yang stokastik selepas mata alat menjadi serpihan menyebabkan amplitud frekuensi ruangan yang lebih rendah daripada frekuensi suapan asas meningkat dengan meruncing. Kaedah CWT didapati lebih efektif untuk mengesan permulaan serpihan mata alat dengan tepat pada masa 16.5 s berbanding 17.13 s yang diperolehi daripada sub-tetingkap FFT. Punca min kuasa dua pekali CWT bagi profil bahan kerja pada skala yang lebih tinggi didapati lebih peka bagi mengesan serpihan mata alat seramik dan seterusnya boleh digunakan sebagai petunjuk untuk mengesan kejadian kegagalan serpihan mata alat seramik.

DETECTION OF CHIPPING IN CERAMIC CUTTING INSERTS FROM WORKPIECE PROFILE SIGNATURE DURING TURNING PROCESS USING MACHINE VISION

ABSTRACT

Ceramic tools are prone to chipping due to their low impact toughness. Tool chipping significantly decreases the surface finish quality and dimensional accuracy of the workpiece. Thus, in-process detection of chipping in ceramic tools is important especially in unattended machining. Existing in-process tool failure detection methods using sensor signals have limitations in detecting tool chipping. The monitoring of tool wear from the workpiece profile using machine vision has great potential to be applied in-process, however no attempt has been made to detect tool chipping. In this work, a vision-based approach has been developed to detect tool chipping in ceramic insert from 2-D workpiece profile signature. The profile of the workpiece surface was captured using a DSLR camera. The surface profile was extracted to sub-pixel accuracy using invariant moment method. The effect of chipping in the ceramic cutting tools on the workpiece profile was investigated using autocorrelation function (ACF) and fast Fourier transform (FFT). Detection of onset tool chipping was conducted by using the sub-window FFT and continuous wavelet transform (CWT). Chipping in the ceramic tool was found to cause the peaks of ACF of the workpiece profile to decrease rapidly as the lag distance increased and deviated significantly from one another at different workpiece rotation angles. From FFT analysis the amplitude of the fundamental feed frequency increases steadily with cutting duration during gradual wear, however, fluctuates significantly after tool has chipped. The stochastic behaviour of the cutting process after tool chipping leads to a sharp increase in the amplitude of spatial frequencies below the fundamental feed frequency. CWT method was found more effective to detect the onset of tool chipping at 16.5 s instead of 17.13 s by sub-window FFT. Root mean square of CWT coefficients for the workpiece profile at higher scale band was found to be more

sensitive to chipping and thus can be used as an indicator to detect the occurrence of the tool chipping in ceramic inserts.

CHAPTER ONE

INTRODUCTION

1.1 Background of the study

Tool condition monitoring plays a significant role in machining process because the worn out cutting tool can be identified and replaced in time to avoid the deterioration in the surface quality and dimension accuracy of the machined part. Flank wear is often selected as the tool life criterion in the tool wear monitoring and is accomplished by direct and indirect methods. Direct tool condition monitoring method is usually performed by means of optical devices such as toolmaker’s microscope, scanning electron microscope (SEM) and CCD (charge coupled device) camera. Toolmaker's microscope and the SEM are the most popular devices used to measure the flank wear in the past. However, these devices have severe limitation as they can only be used in offline measurement which requires the cutting tool to be removed from the machine for inspection and measurement. Numerous previous works have been conducted to measure the flank wear using CCD camera without the need of dismantling the worn tool from machine. However, this method can only be applied between the cutting operations (Lanzetta, 2001; Wang et al., 2006; Zhang et al., 2012; Chethan et al., 2015).

One major prerequisite of an automated manufacturing system is uninterrupted machining to achieve maximum productivity which require continuous monitoring of the cutting process and cutting tool condition. Most of the in-process tool condition monitoring is conducted by indirect methods. Indirect methods of monitoring the tool condition depend upon the measurement of sensor signals, which are indirectly related to the condition of the cutting tool edge. With recent advancement in signal processing technology, a large number of indirect methods have been attempted to achieve the in-process tool wear monitoring based on sensor signal features associated with the tool condition such as cutting force, vibration, acoustic emission (AE) and tool temperature (Rehorn et al., 2005; Teti et al., 2010). Many researchers have even combined several sensors to monitor the multitude of information available during machining to assess the tool condition such as the combination of AE and cutting force (Jemielniak et al., 2011a), cutting force and vibration (Kalvoda & Hwang, 2010), AE and vibration (Bhuiyan et al., 2014), cutting forces, vibration and AE (Jemielniak et al., 2011b), AE and cutting sound (Zhang et al., 2015).

The acquired sensor signal obtained from the machining process has been correlated with flank wear by extracting the signal features from any time domain signal using statistical parameters such as the mean value, the root mean square (RMS), kurtosis and skewness. Sensor signals are also transformed into frequency domain and time-frequency domain. The signal features such as the amplitude of the dominant spectral peaks and wavelet coefficient extracted from these transform are used to correlate to the flank wear (Yesilyurt, 2006; Kious et al., 2010; Fang et al., 2011). Other methods such as statistical regression method, neural network, artificial intelligence and pattern recognition have also been widely explored to establish the correlation between the sensor signal and flank wear (Siddhpura & Paurobally, 2013).

The detection of the tool failure by chipping has become more important recently since hard tools such as ceramic cutting tools are commonly used in the cutting of difficult-to-cut materials such as stainless steel (Lin, 2008; Sobiyi et al., 2015), superalloy (Bushlya et al., 2013), tool steel and hardened tool steel (Özel et al., 2005; Özel et al., 2007; Meddour et al., 2015). Although advances in ceramic processing technology has resulted in high performance tools by improving the toughness, fracture strength and shock resistance, tool chipping and fracture are still serious issues when machining difficult-to-cut material using ceramic cutting tool (Yin et al., 2015). Failure by chipping has more severe effect on the surface finish compared to progressive wear because the cutting forces fluctuates and increases (Liao & Stephenson, 2010). Thus, in-process tool chipping detection as early as possible in ceramic cutting is considered important, in order to stop the machine tool before a catastrophic failure occurs.

Tool chipping occurs when a small piece tool material breaks away from the cutting edge of the tool. The chipped pieces from the cutting edge may vary from microchipping to macrochipping. Breakage of a cutting tool can lead to the total loss of contact between the cutting tool and the workpiece. Chipping and breakage are different from wear which is a gradual process. Chipping and breakage usually occur abruptly resulting in a sudden loss of tool material due to mechanical shocks. The onset of chipping or fracture in a cutting tool results in a change in the contact characteristics between the tool and the workpiece. This in turn results in a significant change in the sensor signals.

Cutting force signal monitoring is one of the most promising methods to detect the precise moment of tool failure. Cutting forces was found to be more effective to detect tool failure than other sensor signals (Li & Mathew,1990). The measurement of cutting force is usually performed by using a dynamometer. When the tool breaks the cutting force increases slightly above the pre-set threshold and then drops sharply because of the loss of contact between the tool and the workpiece (Cakir & Isik, 2005). However, chipping can also cause failure of a cutting edge without decreasing the cutting force significantly when turning of carbon steel using ceramic insert (Jemielniak, 1992). In addition, tool chipping has been reported to be more difficult to detect using cutting force as the variation of cutting force due to tool chipping may not exceed the threshold limits (Shi & Gindy, 2007).

Previous researchers have reported that AE could be used effectively in detecting tool tip chipping. The AE intensity increases as the tool wear increase and a burst AE signal is produced when the cutting tool has chipped (Jemielniak & Othman, 1998; Wang et al., 2003; Belgassim & Jemielniak, 2011). Strong burst in AE was found after tool fracture because of the sudden increase in the contact area between the workpiece and the chipped cutting tool (Lan & Dornfeld, 1984; Wang et al., 2003). However, these results were contradicted by the recent work of Neslušan et al. (2015) who considered that conventional processing of AE signals does not enable the different phases of the tool wear be clearly recognised during turning of bearing steel using ceramic insert. Besides, most AE sensors have been designed for non-destructive testing and are not suitable for tool wear monitoring as they cannot withstand extreme conditions at the cutting point such as high cutting temperatures and impacts from the chip.

The use of sensors fusion allows more reliable tool failure by chipping detection. Sensor signals from different sources are integrated to provide extended information for tool chipping detection such as the combination of AE and motor power (Wang et al., 2003) and AE and cutting force (Balsamo et al., 2016). However, previous study have reported that multiple sensor signals used together produced results a little worse than using a single sensor signal during turning of Inconel 625 using ceramic cutting tool (Jemielniak et al., 2011a).

Direct monitoring methods such as vision and optical approaches have been utilized for tool chipping observation on ceramic cutting tool (Patil & Tilekar, 2014). However, this method is only feasible for in-cycle or intermittent observation which requires the machine to be stopped because the continuous contact between the cutting tool and the workpiece does not allow the capture of images of the cutting tool tip during turning. In order to overcome the limitations of the in-process direct observation on cutting tool, identifying the cutting tool condition by analyzing surface texture of machined surface using digital image processing methods from the images of machined surface has been attempted in the past.

The surface texture of machined surface image contains information about the interaction between the tool and the workpiece such as machining conditions (e.g. feed rate, machining speed), waviness, roughness, vibration and chatter. The machined surface image also carries the information about the cutting tool condition by tool imprint on the workpiece. The surface texture of turned workpiece changes remarkably due to the changes in the cutting tool by wear and chipping. For example, previous study has reported that the groves are even and straight with clear ridge lines when the cutting tool is sharp but the groves appear uneven and ridge lines become disjoint when the cutting tool is dull (Kassim et al., 2007). However, the images of workpiece surface were captured between cutting operation using a CCD camera.

Several attempts have been made to evaluate the tool condition by extracting the surface finish descriptors from the images of the freshly machined surface texture to be correlated with the flank wear (Datta et al., 2013; Dutta et al., 2015). The textural analysis methods showed some potential to interpret the tool condition, but they are subject to the changes in illumination condition and the contamination of the dirt and cutting fluid. In addition, their work was conducted offline and no attempt was made to investigate the correlation between the extracted textures features with tool chipping.

According to machining theory, the surface profile of a turned workpiece is formed by the repetition of the nose radius of the cutting insert at a regular interval of feed rate. Thus, nose radius has direct effect on the surface profile of the workpiece and all predominant tool wear such as the flank wear and notch wear can have significant influence on the surface roughness of the workpiece (Penalva et al., 2002; Grzesik, 2008b). An attempt has been made to determine the nose wear and the flank wear from the silhouette of the workpiece profile captured using CCD camera with the aids of backlighting (Shahabi & Ratnam, 2009a; Shahabi & Ratnam, 2009b). However, the work was carried out in-cycle, i.e. in between cutting process.

The development of an effective in-process tool condition monitoring method to detect the onset of tool chipping has not been attempted by previous researches. The case of tool chipping detection in ceramic cutting tool has not been given great attention by the researchers in the past and this is the motivation of the present study.

1.2 Problem statement

Although the vision method has the advantages of capturing the actual geometric changes arising from the wear and chipping of the cutting tool, the direct assessment of the cutting tool using machine vision is not possible during turning. This is because the cutting area is inaccessible due to the continuous contact between the tool and the workpiece as well as presence of coolant and obstruction by chips during turning operation.

In-process tool chipping monitoring is usually performed by using indirect method based on various sensor signals. However, a number of previous studies have shown that tool chipping is hardly detected using sensor signals due to the significant contradictory findings (Jemielniak, 1992; Wang et al., 2003; Cakir & Isik, 2005; Belgassim & Jemielniak, 2011; Neslušan et al., 2015). Thus, there still exists a need to develop a more reliable in-process tool chipping monitoring method.

Previous studies show that with the advancement in image processing technology, the features extracted from the images of the machined surface texture could be used to correlate well with the cutting tool condition. However, this method requires the machine to be stopped before the images of the machined surface can be captured (Datta et al., 2013; Dutta et al., 2015).

Since the cutting tool tip is directly in contact with the workpiece during the turning operation, an imprint of the cutting tool profile is replicated on the machined surface (Kassim et al., 2007). Therefore, the workpiece profile of turned part is directly dependent on the geometry of the cutting tool tip. As the tool chips, the contact geometry changes, thus affecting the surface being machined. Two dimensional (2-D) image of the surface profile of the turned workpiece has been successfully used for in-cycle nose wear and flank wear measurement in the past (Shahabi & Ratnam, 2009b).

It should be noted from the abovementioned investigations that existing in-process tool condition monitoring method using sensor signals have limitations in detecting tool chipping. The monitoring of tool wear from the turned profile using machine vision shows great potential to be applied in-process. However, to date, no attempt has been made to explore the potential of the 2-D images of the workpiece profile for in-process tool chipping detection in ceramic cutting tool and this has motivated the present study.

1.3 Objectives

The objectives of this research are as follows:

i. To develop a novel approach of in-process tool chipping detection in ceramic cutting insert based on the workpiece profile signature using machine vision.
ii. To investigate the effect of the tool chipping in ceramic cutting inserts on the workpiece profile using autocorrelation function (ACF) and fast Fourier transform (FFT).
iii. To detect the onset of tool chipping by extracting the features from the workpiece profile using sub-window FFT and continuous wavelet transform (CWT).

1.4 Research approach

The approaches of this study are as follows:

i. A 2-D machine vision system consisting of a digital single lens reflex (DSLR) camera and backlighting was developed to capture the images of the edge of the turned workpiece.

ii. Experiments were carried out using aluminium oxide based ceramic cutting insert and the workpiece materials were AISI 01 Arne oil hardening tool steel and SUS 304 stainless steel with diameter of 50 mm.

iii. The condition of the cutting insert was evaluated using the SEM.

iv. Invariant moment method was used to extract the workpiece profile.

v. ACF, FFT and CWT were utilised to extract the features from the 2-D workpiece profile that correlate to tool chipping.

1.5 Scope of study

The scopes of this research are as follows:

i. Proposed tool chipping detection method only considers in turning process.

ii. This study focuses on the tool chipping detection in the aluminium oxide based ceramic cutting insert.

iii. This study distinguishes the sign of tool chipping from gradual wear using 2-D images of turned workpiece.

1.6 Organization of thesis

This thesis is organized into five chapters. The overview of the research is presented in the Chapter One. The background of the research and the existing problems in similar studies are addressed. The objectives, research approach and the scopes of the research are listed. Chapter Two is about the literature review focusing on the in-process tool condition monitoring methods. The advantages and limitations of the existing in-process tool condition monitoring methods are discussed in detailed. Literature reviews reveal that an effective in-process tool chipping detection methods in ceramic cutting insert has not been thoroughly investigated.

The methodology for in-process detection of tool failure by chipping from the 2-D workpiece profile signature using machine vision method is outlined in Chapter Three. The proposed vision system using high resolution digital camera at high shutter speed has been used in this study for capturing the images of the workpiece profile during turning operation is presented. Detailed workpiece profile extraction method from 2-D images of the workpiece up to sub-pixel accuracy is described in this chapter. Finally, analysis of the 2-D workpiece profile to detect the tool chipping is discussed. The specific procedures in detection of tool chipping in ceramic cutting insert based on the 2-D surface profile extracted from the images of the edge of turned workpiece using ACF, FFT and CWT are discussed.

The results of the simulations and experiments are described in Chapter Four. The effects of the tool chipping on the workpiece surface are discussed. The results on detection of tool chipping in ceramic cutting insert from workpiece profile signature using vision method is presented. Finally, Chapter Five provides conclusion of the thesis and recommendations for future work. The contributions of the proposed method in the field of tool chipping detection are also presented.

CHAPTER TWO

LITERATURE REVIEW

2.1 Introduction

A review of previous research works that are closely related to the studies on the tool failure monitoring in a turning process is presented in this chapter. Firstly, types of tool failure are presented. Previous research works related to the monitoring of tool failure by gradual wear and premature failure by chipping are reviewed in the next section. Emphasis is placed on the in-process detection of the tool chipping for ceramic cutting tool. A summary of the literature review is presented at the end of the chapter.

2.2 Types of tool failure

The turning process is widely used in industry for finish machining of a wide range of components. Tool failure monitoring in turning is essential to achieve not only optimum productivity by reducing machine downtime and unnecessary tool changes, but also to obtain high surface quality and dimensional accuracy as well as minimize the damage to the workpiece or machine tool.

Tool failure can be classified into two groups namely wear and fracture. Wear is generally the removal of material from a cutting tool and is a result of the relative motion between the tool and workpiece. Flank wear at the front edge of the tool flank face and crater wear at the tool rake face are the most typical modes of tool wear in turning (Figure 2.1). Flank wear is mainly caused by the abrasion between the workpiece and the cutting tool. Crater wear is the formation of a groove on the tool rake face where the chips rubs the tool surface.

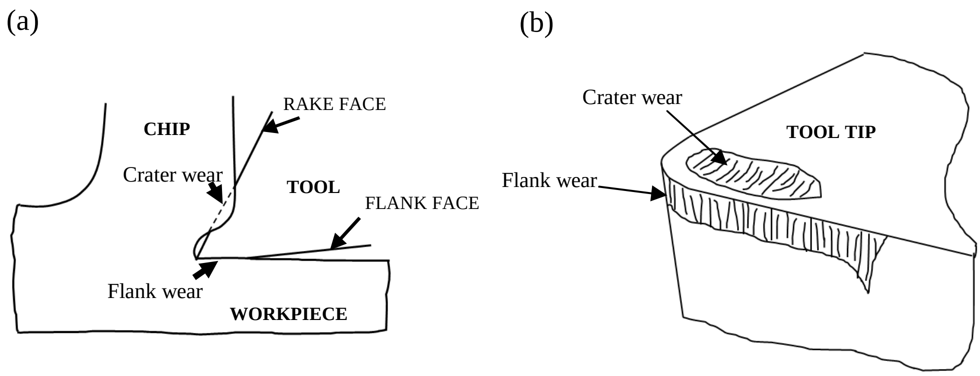

Figure 2.1: (a) Tool-workpiece interaction, and (b) location of crater wear and flank wear (Özel & Davim, 2009)

Directly measured dimensional features of a typical wear pattern have been applied in the past to assess cutting tool's performance which are standardized in International Organization for Standardization (ISO, 1993). Compared to crater wear, flank wear is often used as a criterion to define the end of effective tool life as the wear progresses gradually as shown in Figure 2.2 and thus can be easily monitored.

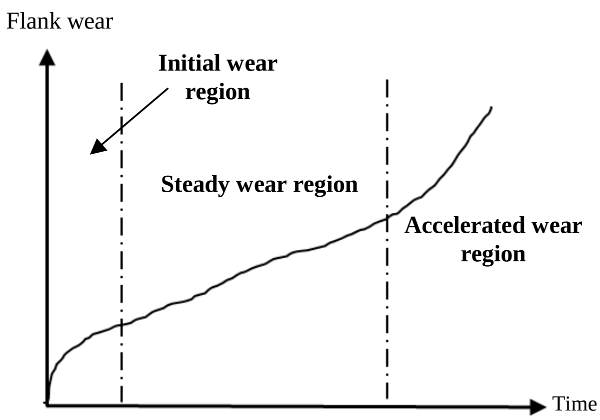

Figure 2.2: Typical flank wear versus time curve (Wang & Gao, 2006)

Flank wear appears in the wear land and is defined by the width of the wear land VB as shown in the Figure 2.3. According to the ISO (1993), the cutting tool is considered to have failed if the average flank wear (VB_B) and the maximum flank wear (VB_{max}) exceeds some critical value such as VB_B> 0.3 mm and VB_{max}> 0.6 mm.

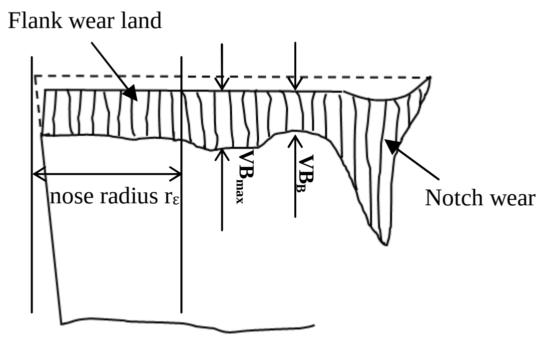

Figure 2.3: Typical wear pattern according to ISO (1993)

Tool fracture is the damage on the cutting edge that range from microchipping to gross chipping. Premature tool failure by chipping refers to the breaking away of small piece from the edge of a cutting tool in micro-scale to massive chipping of cutting edge as shown in Figure 2.4(a) and Figure 2.4(b) respectively. Tool breakage, on the other hand, is the breaking of the entire insert that leads to a total loss of contact between the cutting edge and workpiece as shown in Figure 2.4(c). Chipping of a tool is different from wear, which is a gradual process, premature tool failure by chipping and breakage mostly occur as a sudden and unpredictable breaking away of tool material from the cutting edge. The main reasons for chipping and breakage include brittle nature of the cutting tool materials, the rapid growth of the crater wear, pre-existing potential cracks on the cutting edge, inclusions in the workpiece profile leading to mechanical shocks and impact loading resulting from the sudden engagement of the cutting tool into the workpiece (Grzesik, 2008a).

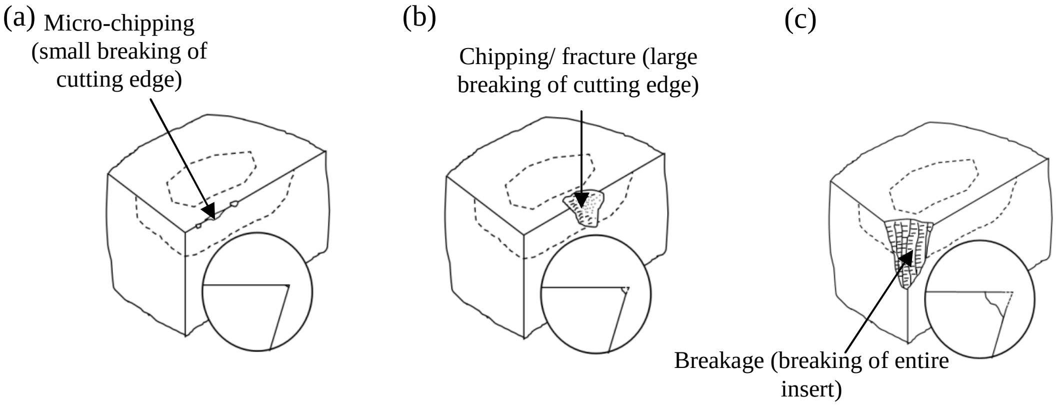

Figure 2.4: Tool failure by chipping and breakage (Grzesik, 2008a)

2.3 Monitoring of gradual wear

Monitoring of gradual wear generally can be divided into two types: direct and indirect method which is explained in Section 2.3.1 and Section 2.3.2, respectively.

2.3.1 Monitoring of gradual wear using direct method

Extensive efforts have been focused on tool wear monitoring using optical methods which is conducted by directly analysing the change in the geometry of the cutting tool. Toolmaker's microscope is the most popular device used to measure wear of cutting tools (Grzesik, 2008a; Čerče et al., 2015). SEM with magnification in the range of several hundred to several thousand is most often used for micro examination. More advanced measuring techniques such as white light interferometry and confocal microscope can be of interest when the analysis in the nano-scale range is necessary and is useful for crater wear measurement (Devillez et al., 2004; Dawson & Kurfess, 2005). However, the abovementioned direct methods have one main limitation, which is they can only be used for offline measurement. For the offline measurement, the cutting tool has to be dismantled from the machine tool for inspection and this causes interruption to the cutting process as well as is time consuming. Atomic force microscopes (AFM) are powerful tools for 3-D profile measurement with a very high resolution. However, it is very difficult and time consuming to accurately align the AFM cantilever probe with respect to the cutting edge (Cazaux, 2004; Mazzeo et al., 2009).

The past decades has seen the rapid development of tool condition monitoring using machine vision coupled with image processing techniques as direct method in flank wear measurement. In this method, a CCD camera with appropriate lighting reflected in the plane of wear surface is used to acquire the image of the cutting tool. Kurada and Bradley (1997) carried out pioneering work in direct tool condition monitoring by capturing images of flank wear using two fibre optic guided lights and CCD camera. Lanzetta (2001) recognized the types of defects of cutting tool and simultaneously measured the flank wear using a CCD camera equipped with an auto-focus zoom lens for different sizes of cutting tool. However, their study was performed offline.

Pfeifer and Weigers (2000) captured images of tool inserts using CCD camera with a ring light in different angles of incidence for controlled illumination. But there still remain the problem of accuracy because the measurement of flank wear using digital image processing method is highly dependent on the quality of captured images as it is vary considerably although there is a small variation in illumination. This leads to error in dimensional measurements. Sortino (2003) developed an automated flank wear measurement software by using statistical filtering method from a colour image. However, this measurement method is limited for small flank wear width.

Jurkovic et al. (2005) proposed a vision system which comprised of a CCD camera, laser diod with linear projection as a light, frame grabber for capturing and a personal computer as direct means in flank wear and crater wear measurement. Castejón et al. (2007) and Barreiro et al. (2008) applied machine vision to determine flank wear by means of the discriminant analysis based on geometrical descriptors. The main advantages of their methods is the information about the condition of cutting tool can be obtained without having to remove the cutting inserts from the tool holders. However, the proposed wear measurement techniques using machine vision method were performed between the cutting operation such as in-cycle or intermittent, which requires the machine tool to be stopped. Fadare and Oni (2009) used Canny edge operator to detect significant edges of the worn area of a cutting tool in order to determine the flank wear and notch wear. Although this method is very useful for flank wear determination, but the method is very much sensitive to the fluctuation of ambient light.

Nose wear measurement has also gained attention in the recent years since the machined surface is mainly formed by the tool nose in finish turning. The nose wear can be measured by subtracting the 2-D image of a worn tool from the image of an unworn tool. Kwon and Fischer (2003) determined the nose wear by subtracting the worn tool image from a template after spatial registration of these images. A similar method was also carried out by Shahabi and Ratnam (2009a). The nose wear was determined by subtracting the 2-D image of a worn tool from the image of unworn tool. The subtraction method can effectively and accurately determine the nose wear, but it requires two images that are aligned precisely before the subtraction. To overcome the limitation, a new approach was proposed by Mook et al. (2009) for measuring nose wear using a single worn cutting tool image. However, this method is not feasible to implement in-process.

In a recent work, Čerče et al. (2015) developed an intermittent 3-D cutting tool wear measurement system using a 2-D profile laser displacement sensor. With movement of the laser displacement sensor across the cutting insert, the sensor measured the distance from the measurement head to the points projected onto the cutting insert and the profile data of cutting insert were grabbed in a matrix form for further evaluation. The depth of flank wear is clearly visible from the comparison of the new and worn cutting inserts cross-sections profiles. Nose wear and crater wear can also be determined by calculating tool wear volume. However, the disadvantage of this method is that it is sensitive to contaminants such as coolant, chips and dust that may remain on the cutting inserts to be measured, which can cause error in the measurement. Chethan et al. (2015) used digital camera with a halogen light to capture the images of cutting insert. The wear region of the cutting insert was estimated using Blob analysis in order to extract the features such as wear area, perimeter and compactness to correlate with the flank wear. However, this method was carried out offline.

2.3.2 Monitoring of gradual wear using indirect method

In-process tool wear monitoring is gaining considerable importance in the manufacturing industry. This can be attributed to the transformation of manufacturing systems from manually operated production machines to highly automated machining centres. In-process tool condition monitoring implies identifying the cutting tool conditions without interrupting the machining process. The direct tool wear evaluation on cutting tool using machine vision system is very simple and accurate, but this method only can be implemented in between cutting operations when the cutting tool is not in contact with the workpiece.

In-process monitoring of tool wear is usually performed by indirect methods that depend upon the measurement of sensor signals which are indirectly correlated to the condition of the cutting tool during the machining operation. Commonly used sensor signal in previous studies including cutting force, AE, vibration, temperature, motor current and power consumption.

Cutting force has been proven to be the one of the significant indicator of tool wear as gradual increase in tool wear during machining causes the cutting force to increase (Gao et al., 2015). The cutting forces generally increases with flank wear because an increase in contact area of the wear land with the workpiece. The use of dynamometer is the most popular method for measurement of cutting forces. It was reported that cutting force currently is the most reliable method employed in in-process tool wear monitoring because cutting force is more sensitive to tool wear than AE and vibration. Thus, many studies have been conducted in the past using cutting forces to establish the relationship with the flank wear (Sikdar & Chen, 2002; Sick, 2002; Oraby et al., 2005).

Dimla and Lister (2000) used three perpendicular cutting forces to correlate with the flank wear through time series and FFT. They reported that the tangential cutting force is the most sensitive to flank wear while Li (2005) reported that the feed and radial forces are more sensitive to flank wear than tangential cutting force. Fang et al. (2011) concluded that feed force was more sensitive to flank wear. Salgado and Alonso (2007) also found that feed force was more suitable to be applied in tool wear monitoring system because the radial force and tangential force showed greater error in flank wear estimation which reduce the success rate and can cause false alarm. Zhou et al. (2003) indicated that the radial force showed a significant increase when the flank wear increase to 0.2 mm. Penedo et al. (2012) also suggested the radial cutting force to monitor the flank wear by using a hybrid incremental model. In a recent work, Liao et al. (2016) developed a novel approach for flank wear monitoring which is based on the multi-scale hybrid hidden Markov model analysis of cutting force signal. In their study, the instantaneous resultant forces was taken into account because the authors indicated that resultant force signal provides multi-scale information of different directions.

Cutting forces are often used to monitor the flank wear because cutting forces are easy to measure and they have a clear phenomenological relationship with flank wear. However, there is no agreement to which cutting force component has more closer relationship with tool wear. In addition, Liao et al. (2016) reported that the high temperature in tool tip and fast tool material losing rate always result in rapid tool wear and large fluctuation of cutting force during machining of difficult-to-cut materials.

Ren et al. (2011) applied cutting forces in a Takagi-Sugeno-Kang (TSK) fuzzy approach for tool wear monitoring. Liu et al. (2013a) used several statistical parameters such as average value, RMS, kurtosis and skewness extracted from the cutting forces as input of back-propagation neural network and adaptive neuro-fuzzy inference system for in-process flank wear monitoring. In a recent work, Gao et al. (2015) proposed a data driven modeling framework for flank wear monitoring in turning which is based on statistical processing of cutting force wavelet transform by a hidden Markov tree model. The drawback of these methods is greater computational burden in training phase as a large number of observation samples were used as training data with different machining conditions to build the model to estimate the flank wear.

Ghani et al. (2009) presented a tool wear monitoring method from the cutting forces and cutting parameters using the regression model to predict the flank wear. Camargo et al. (2014) developed a mathematical model based on multiple regression analysis to estimate tool wear during turning of AISI D6 hardened steel using PCBN cutting insert. Although the developed regression model accurately determined the flank wear, the regression based method cannot be extrapolated to different range of cutting condition and to other workpiece and cutting tool materials.

Monitoring cutting tool wear via AE signal analysis has long been practiced. AE can be defined as the transient elastic wave generated by the sudden release of energy in a material. There are several sources of AE signal during machining such as (i) friction contact between the flank face of cutting tool and workpiece resulting in flank wear, (ii) plastic deformation of cutting tool, (iii) chipping and tool fracture (Li, 2002). The main benefit in the use of AE signal in tool wear monitoring is that the frequency range of the AE signal is much higher than that of the machine vibrations and environmental noises.

Bhaskaran et al. (2012) used skewness and kurtosis of the RMS value of AE signal to monitor flank wear. The kurtosis of RMS value of AE signal increased as the flank wear increased. High skewness of the RMS value of AE signal was found when the flank wear land reached the critical value. Compared to the conventional data processing method, Chen and Li (2007) reported that the wavelet resolution coefficient norm of AE signal is more reliable and useful to estimate tool wear. However, low magnitude of AE signal was generated when the cutting tool undergoes gradual wear compared to the higher magnitude of AE signals which accompanies tool failure by plastic deformation or tool chipping. Thus, AE is not suitable for use as tool wear indicator in gradual wear monitoring applications, but could be used to detect the end of tool life when the tool has deformed due to the excessive wear.

Maia et al. (2015) reported that monitoring the tool wear through the AE signal processed using the average power spectral density (PSD) is sensitive to the wear rate, responding with the high magnitude AE signal value at the beginning of tool life and followed by a decrease at the middle of tool life and increase at the end of the tool life when the wear rate becomes higher. However, monitoring of tool wear using AE signal was difficult because each of the mild wear and severe wear excited a different frequency band (Hase et al., 2012).

During machining, the workpiece and chips rub against the worn tool and produce vibrations which can be used in various ways for tool wear monitoring. Accelerometers are often used to acquire the vibration response. Dimla (2002) reported that vibration increased with flank wear and the vibration signal in the feed and tangential direction were the most sensitive to flank wear. The results showed that time domain analysis of vibration signal to be more sensitive to cutting condition than tool wear, whereas sum total power of vibration signal correlated well with the flank wear. However, the author found that vibration signal can only give better estimation of flank wear in low feed rate because the vibration signal is noisier in higher feed rate.

Chen et al. (2011) monitored flank wear in turning based on logistic regression model by using vibration signals. The wavelet package transform was used to decompose the original vibration signal to find out the frequency bands which well correlated to flank wear and applied the extracted most related features of vibration signals into the logistic regression model to monitor the cutting tool wear. Alonso and Salgado (2008) proposed tool wear monitoring based on longitudinal and transverse vibration signal using singular spectrum analysis (SSA) to decompose the acquired vibration signal. The RMS and variance of the decomposed vibration signals were extracted and the corresponding cutting condition parameters were fed into a back-propagation neural network to determine the flank wear. However, not all the decomposed vibration signals correlated well with the flank wear. The information in the decomposed vibration signals about flank wear is contained mostly in the high frequency components. Alonso and Salgado (2008) indicated that the range of frequencies most correlated with the tool wear changes with the cutting tool condition and tool wear. For this reason, implementation of the tool condition monitoring based on vibration signal becomes difficult because the frequency range that correlated with the tool wear was difficult to be identified.

Temperature has also been used as a parameter for monitoring tool wear because heat generation is unavoidable in all machining process and it will damage the cutting tool tip due to the effect of diffusion and plastic deformation. Several attempts have been made to monitor the wear of cutting tool based on temperature monitoring. To measure the temperature in the tool tips, thermocouples are the commonly used sensors (O'Sullivan & Cotterell, 2001; Choudhury & Bartarya, 2003; Korkut et al., 2011). However, due to the narrow shear band, chips obstruction and the contact phenomenon between tool and workpiece the measurement of the cutting temperatures closed to tool tip becomes much difficult. In addition, since the temperature varies during machining and cannot be uniquely described by discrete values at a point this can cause error in the tool wear estimation (Sivasakthivel & Sudhakaran, 2013). Infrared thermal cameras have been applied to overcome the limitation of the thermocouple (O'Sullivan & Cotterell, 2001; Davoodi & Hosseinzadeh, 2012). However, the major drawback of the infrared sensor is due the coolant and the chip that may come between the sensor and the surface to be measured thereby causing errors in measurement.

Application of microphone to measure the sound signal for tool condition monitoring has also been attempted in the past. Tekiner and Yesilyurt (2004) used sound signal to assess the flank wear, built up edge, radii of chip curl and surface roughness. Salgado and Alonso (2007) estimated flank wear progression by the emitted sound using singular spectrum analysis in turning of AISI 1040 steel. Samraj et al. (2011) used singular value decomposition to extract the information regarding flank wear from the emitted sound during turning. Monitoring of flank wear using sound signal has been proven possible, however this method is difficult to implement in the real industry because the noise from adjacent machines and motors can influence the signals.

The use of current and power signal has also been proposed in tool wear monitoring, either from spindle motor or from feed motor. This is because a worn cutting tool require more cutting forces than an unworn cutting tool, thus resulting in more power and current. The major advantage of using current and power signals is its simple hardware implementation that does not interfere with the cutting process. However, current and power signals are not as sensitive to flank wear when compared to cutting forces, AE and vibration signal (Kaye et al., 1995; Silva et al., 1998; Fu & Hope, 2006; Lee et al., 2007).

The need for a more reliable and accurate tool condition monitoring system over a wide range of industrial application is driving the research works towards a multiple sensor approach (known as sensor fusion). This is because signals from a single type of sensor are typically insufficient to provide enough information for tool wear monitoring. The use of several sensors at different locations simultaneously has been proposed for data acquisition in the past. Signals from different sensors are integrated to give the maximum information needed about the tool wear such as the combination of cutting force and vibration (Chelladurai et al., 2008; Chen et al., 2010; Fang et al., 2011), AE and cutting force (Youn et al., 1994; Jemielniak et al., 2011a), AE and vibration (Bhuiyan et al., 2014), cutting forces, vibration and AE (Jemielniak et al., 2011b; Gajate et al., 2012), AE and cutting sound (Zhang et al., 2015).

REFERENCES

Abellan-Nebot, J.V., & Subirón, F.R. (2010). A review of machining monitoring systems based on artificial intelligence process models. *International Journal of Advanced Manufacturing Technology, 47(1),* 237-257.

Aich, U., & Banerjee, S. (2017). Characterizing topography of EDM generated surface by time series and autocorrelation function. *Tribology International, 111,* 73-90.

Alonso, F.J., & Salgado, D.R. (2008). Analysis of the structure of vibration signals for tool wear detection. *Mechanical Systems and Signal Processing, 22(3),* 735-748.

ASME B46.1 (2009) *Surface texture (surface roughness, waviness and lay).* The American Society of Mechanical Engineers: New York.

Azhar, A.Z.A., Mohamed, H., Ratnam, M.M., & Ahmad, Z.A. (2010). The effects of MgO addition on microstructure, mechanical properties and wear performance of zirconia-toughened alumina cutting inserts. *Journal of Alloys and Compounds, 497(1-2),* 316-320.

Babouri, M.K., Ouelaa, N., & Djebala, A. (2016). Experimental study of tool life transition and wear monitoring in turning operation using a hybrid method based on wavelet multi-resolution analysis and empirical mode decomposition. *International Journal of Advanced Manufacturing Technology, 82(9),* 2017-2028.

Balsamo, V., Caggiano, A., Jemielniak, K., Kossakowska, J., Nejman, M., & Teti, R. (2016). Multi sensor signal processing for catastrophic tool failure detection in turning. *Procedia CIRP, 41,* 939-944.

Barreiro, J., Castejón, M., Alegre, E., & Hernandez, L.K. (2008). Use of descriptors based on moments from digital images for tool wear monitoring. *International Journal of Machine Tools and Manufacture, 48(9),* 1005-1013.

Belgassim, O., & Jemielniak, K. (2011). Tool failure detection based on statistical analysis of metal cutting acoustic emission signals. *World Academy of Science, Engineering and Technology, 50(2),* 545-552.

Bendat, J.S., & Piersol, A.G. (1993). *Engineering application of correlation and spectral analysis.* New York: Wiley.

Bhaskaran, J., Murugan, M., Balashanmugam, N., & Chellamalai, M. (2012). Monitoring of hard turning using acoustic emission signal. *Journal of Mechanical Science and Technology, 26(2),* 609-615.

Bhuiyan, M.S.H., Choudhury, I.A., & Dahari, M. (2014). Monitoring the tool wear, surface roughness and chip formation occurrences using multiple sensors in turning. *Journal of Manufacturing Systems, 33(4),* 476-487.

Binsaeid, S., Asfour, S., Cho, S., & Onar, A. (2009). Machine ensemble approach for simultaneous detection of transient and gradual abnormalities in end milling using multisensor fusion. *Journal of Materials Processing Technology, 209(10),* 4728-4738.

Boryczko, A. (2011). Profile irregularities of turned surfaces as a result of machine tool interactions. *Metrology and Measurement Systems, 18(4),* 691-700.

Bushlya, V., Zhou, J.M., Avdovic, P., & Ståhl, J.E. (2013). Performance and wear mechanisms of whisker-reinforced alumina, coated and uncoated PCBN tools when high-speed turning aged Inconel 718. *International Journal of Advanced Manufacturing Technology, 66(9),* 2013–2021.

Cakan, A. (2011). Real-time monitoring of flank wear behavior of ceramic cutting tool in turning hardened steels. *International Journal of Advanced Manufacturing Technology, 52(9),* 897-903.

Cakir, M.K., & Isik, Y. (2005). Detecting tool breakage in turning AISI 1050 steel using coated and uncoated cutting tools. *Journal of Materials Processing Technology, 159(2),* 191-198.

Camargo, J.C., Dominguez, D.S., Ezugwu, E.O., & Machado, A.R. (2014). Wear model in turning of hardened steel with PCBN tool. *International Journal of Refractory Metals and Hard Materials, 47,* 61-70.

Castejón, M., Alegre, E., Barreiro, J., & Hernández, L.K. (2007). Online tool wear monitoring using Geometric Descriptors from digital images. *International Journal of Machine Tools and Manufacture, 47(12-13),* 1847-1853.

Cazaux, J. (2004). Errors in nanometrology by SEM. *Nanotechnology, 15(9),* 1195-1199.

Čerče, L., Pušavec, F., & Kopač, J. (2015). 3D cutting tool wear monitoring in the process. *Journal of Mechanical Science and Technology, 29(9),* 3885-3895.

Chelladurai, H., Jain, V., & Vyas, N. (2008). Development of a cutting tool condition monitoring system for high speed turning operation by vibration and strain analysis. *International Journal of Advanced Manufacturing Technology, 37(5),* 471-485.

Chen, B., Chen, X., Li, B., He, Z., Cao, H., & Cai, G. (2011). Reliability estimation for cutting tools based on logistic regression model using vibration signals. *Mechanical Systems and Signal Processing, 25(7),* 2526-2537.

Chen, H., Huang, S., Li, D., & Fu, P. (2010). Turning tool wear monitoring based on fuzzy cluster analysis. In Zeng, Z., & Wang, J. (Eds.), *Advances in Neural Network Research and Application* (pp. 739-745). Berlin: Springer.

Chen, Q., Yang, S., & Li, Z. (1999). Surface roughness evaluation by using wavelets analysis. *Precision Engineering, 23(3),* 209–212.

Chen, X., & Li, B. (2007). Acoustic emission method for tool condition monitoring based on wavelet analysis. *International Journal of Advanced Manufacturing Technology, 33(9),* 968-976.

Chen, Y.L., Cai, Y., Shimizu, Y., Ito, S., Gao, W., & Ju, B.F. (2016). On-machine measurement of microtool wear and cutting edge chipping using a diamond edge artifact. *Precision Engineering, 43,* 462-467.

Chethan, Y.D., Ravindra, H.V., Krishne, Y.T., & Kumar, S.B. (2015). Machine vision for tool status monitoring in Inconel 718 using Blob analysis. *Materials Today: Proceeding, 2(4-5),* 1841-1848.

Cheung, C.F., & Lee, W.B. (2000). A multi-spectrum analysis of surface roughness formation in ultra-precision machining. *Precision Engineering, 24(1),* 77-87.

Choudhury, S.K., & Bartarya, G. (2003). Role of temperature and surface finish in prediction tool wear using neural network and design of experiment. *International Journal of Machine Tools Manufacture, 43(7),* 747-753.

Colgan, J., Chin, H., Danai, K., & Hayashi, S.R. (1994). On-line tool breakage detection in turning: A multi-sensor method. *Journal of Engineering for Industry, 116(1),* 117-123.

Datta, A., Dutta, S., Pal, S.K., & Sen, R. (2013). Progressive cutting tool wear detection from machined surface images using Voronoi tessellation method. *Journal of Materials Processing Technology, 213(12),* 2339-2349.

Daubeches, I. (1990). The wavelet transformation, time-frequency localization and signal analysis. *IEEE Transactions on Information Theory, 36(5),* 961-1005.

Davoodi, B., & Hosseinzadeh, H. (2012). A new method for heat measurement during high speed machining. *Measurement, 45(8),* 2135-2140.

Dawson, T.G., & Kurfess, T.R. (2005). Quantification of tool wear using light interferometry and three dimensional computational metrology. *International Journal of Machine Tool and Manufacture, 45(4-5),* 591-596.

Devillez, A., Lesko, S., & Mozerc, W. (2004). Cutting tool crater wear measurement with white light interferometry. *Wear, 256(1-2),* 56-65.

Dimla, D.E. (2002). The correlation of vibration signal features to cutting tool wear in a metal turning operation. *International Journal of Advanced Manufacturing Technology, 19(10),* 705-713.

Dimla, D.E., & Lister, P.M. (2000). Online metal cutting tool condition monitoring. I: force and vibration analysis. *International Journal of Machine Tools and Manufacture, 40(5),* 739-768.

Dutta, S., Datta, A., Chakladar, N.D., Pal, S.K., Mukhopadhyay, S., & Sen, R. (2012). Detection of tool condition from the turned surface images using an accurate grey level co-occurrence technique. *Precision Engineering, 36(3),* 458-466.

Dutta, S., Pal, S.K., & Sen, R. (2015). Tool condition monitoring in turning by applying machine vision. *Journal of Manufacturing Science and Engineering, 138(5),* 1-17.

Dutta, S., Pal, S.K., & Sen, R. (2016). On-machine tool prediction of flank wear from machined surface images using texture analyses and support vector regression. *Precision Engineering, 43,* 34-42.

Fadare, D.A., & Oni, A.O. (2009). Development and application of a machine vision system for measurement of tool wear. *ARPN Journal of Engineering and Applied Science, 4(4),* 42-49.

Fang, N., Srinivasa, P., & Mosquea, S. (2011). Effect of tool edge wear on the cutting forces and vibration in high-speed finish machining of Inconel 718: an experimental study and wavelet transform analysis. *International Journal of Advanced Manufacturing Technology, 52(1),* 65-77.

Fang, N., Pai, P.S., & Edwards, N. (2012). Tool-edge wear and wavelet packet transform analysis in high speed machining of Inconel 718. *Journal of Mechanical Engineering, 58(3),* 191-202.

Feng, Z., Liang, M., & Chu, F. (2013). Recent advances in time-frequency analysis methods for machinery fault diagnosis: A review with application examples. *Mechanical Systems and Signal Processing, 38(1),* 165-205.

Fu, P. & Hope, A.D. (2006). *The application of B-spline neurofuzzy network for condition monitoring of metal cutting tool.* Paper presented at PRICAI 2006: Trends in Artificial Intelligence, 9th Pacific Rim International Conference on Artificial Intelligence, Guilin China.

Gajate, A., Haber, R., Toro, R., Vega, P., & Bustillo, A. (2012). Tool wear monitoring using neuro-fuzzy techniques: a comparative study in a turning process. *Journal of Intelligent Manufacturing, 23(3),* 869-882.

Gao, D., Liao, Z.R., Lv, Z.K., & Lu, Y. (2015). Multi-scale statistical signal processing of cutting force in cutting tool condition monitoring. *International Journal of Advanced Manufacturing Technology, 80(9),* 1843-1853.

Gao, R.X., & Yan, R. (2010). From Fourier Transform to Wavelet Transform: A Historical Perspective. In R.X. Gao, & R. Yan (Eds.), *Wavelet: Theory and Application for Manufacturing,* (pp.17-32). United States: Springer.

Ghani, J.A., Rizal, M., Sayuti, A., Nuawi, M.Z., Rahman, M.N., & Haron, C.H.C. (2009). New regression model and I-Kaz method for online cutting tool wear monitoring. *World Academy of Science, Engineering and Technology, 60,* 420-425.

Gong, W., Obikawa, T., & Shirakashi, T. (1997). Monitoring of tool wear states in turning based on wavelet analysis. *JSME International Journal Series C Mechanical Systems, Machine Elements and Manufacturing, 40(3),* 447-453..

Grzesik, W. (2008a) *Advanced Machining Processes of Metallic Materials*. Oxford, UK: Elsevier Publications.

Grzesik, W. (2008b) Influence of tool wear on surface roughness in hard turning using differently shaped ceramic tools. *Wear, 265(3-4),* 327-335.

Grzesik, W., & Brol, S. (2009). Wavelet and fractal approach to surface roughness characterization after finish turning of different workpiece materials. *Journal of Materials Processing Technology, 209(5),* 2522-2531.

Grzesik, W., & Zalisz, Z. (2008). Wear phenomenon in the hard steel machining using ceramic cutting tool. *Tribology International, 41,* 802-812.

Guo, Y.B., & Ammula, S.C. (2005) Real-time acoustic emission monitoring for surface damage in hard machining. *International Journal of Machine Tools and Manufacture, 45(14),* 1622-1627.

Haddadi, E., Shabghard, M.R., & Ettefagh, M.M. (2008). Effect of different tool edge condition on wear detection by vibration spectrum analysis in turning operation. *Journal of Applied Sciences, 8(21),* 3879-3886.

Hase, A., Mishina, H., & Wada, M. (2012). Correlation between features of acoustic emission signals and mechanical wear mechanisms. *Wear, 292-293,* 144-150.

International Organization for Standardization. (1993). *ISO 3685: Tool-life testing with single-point turning tools*. Retrieved from: https://www.asme.org/products/ codes-standard/b461-2009-surface-texture-surface-roughness

Jemielniak, K. (1992). Detection of cutting edge breakage in turning. *CIRP Annals, 41(1),* 97-100.

Jemielniak, K., Kossakowska, J., & Urbanski, T. (2011a). Application of wavelet transform of acoustic emission and cutting force signals for tool condition monitoring in rough turning of Inconel 625. *Proceedings of the Institution of Mechanical Engineers, Part B: Journal of Engineering Manufacture, 225(1),* 123-129.

Jemielniak, K., & Othman, O. (1998). Tool failure detection based on analysis of acoustic emission signals. *Journal of Materials Processing Technology, 76(1-3),* 192-197.

Jemielniak, K., & Szafarczyk, M. (1992). Detection of cutting edge breakage in turning. *CIRP Annals-Manufacturing Technology, 41(1),* 97-100.

Jemielniak, K., Urbański, T., Kossakowska, J., & Bombiński, S. (2011b). Tool condition monitoring based on numerous signal features. *International Journal Advanced Manufacturing Technology, 59(1),* 73-81.

Jiang, C.Y., Zhang, Y.Z., & Xu, H.J. (1987). In-process monitoring of tool wear stage by the frequency band energy method. *CIRP Annals-Manufacturing Technology,36(1),* 45-48.

Josso, B., Burton, D.R., & Lalor, M.J. (2002). Frequency normalised wavelet transform for surface roughness analysis and characterisation. *Wear, 252(5-6),* 491-500.

Jurkovic, J., Korosec, M., & Kopac, J. (2005). New approach in tool wear measuring technique using CCD vision system. *International Journal of Machine Tools and Manufacture 45(9):* 1023-1030.

Kalvoda, T., & Hwang, Y.R. (2010). Analysis of signal for monitoring of nonlinear and non-stationary machining process. *Sensors and Actuators A, 161(1-2),* 39-45.

Kassim, A.A., Mannan, M.A., & Mian, Z. (2007). Texture analysis methods for tool condition monitoring. *Image and Vision Computing, 25(7),* 1080-1090.

Kaye, J.E., Yan, D.H., Popplewell, N., & Balakrishnan, S. (1995). Predicting tool flank wear using spindle speed change. *International Journal of Machine Tools and Manufacture, 35(9),* 1309-1320.

Khraisheh, M.K., Pezeshki, C., & Bayoumi, A.E. (1995). Time series based analysis for primary chatter in metal cutting. *Journal of Sound and Vibration, 180(1),* 67-87.

Kim, J.D., & Choi, I.H. (1996). Development of a tool failure detection system using multi-sensors. *International Journal of Machine Tools and Manufacture, 36(8),* 861-870.

Kious, M., Ouahabi, A., Boudraa, M., Serra, R., & Cheknane, A. (2010). Detection process approach of tool wear in high speed milling. *Measurement, 43(10),* 1439-1446.

Korkut, I., Acir, A., & Boy, A. (2011). Application of regression and artificial neural network analysis in modeling of tool-chip interface temperature in machining. *Expert System with Applications, 38(9),* 11651-11656.

Kurada, S., & Bradley, C. (1997). A machine vision system for tool wear assessment. *Tribology International, 30(4),* 295-304.

Kwak, J.S. (2006). Application of wavelet transform technique to detect tool failure in turning operation. *International Journal of Advanced Manufacturing Technology, 28(11),* 1078-1083.

Kwon, Y., & Fischer, G.W. (2003). A novel approach to quantifying tool wear and tool life managements for optimal tool management. *International Journal of Machine Tools and Manufacture, 43(4),*359-368.

Lan, M.S., & Dornfeld, D.A. (1984). In-process tool fracture detection. *Journal of Engineering Materials and Technology, 106(2),* 111-118.

Lanzetta, M. (2001). A new flexible high resolution vision sensor for tool condition monitoring. *Journal of Materials Processing Technology, 119(1-3),* 73-82.

Lauro, C.H., Brandao, L.C., Baldo, D., Reis, R.A., & Davim, J.P. (2014). Monitoring and processing signal applied in machining process-A review. *Measurement, 58,* 73-86.

Leavey, C.M., James, M.N., Summerscales, J., & Sutton, R. (2003). An introduction to wavelet transforms: a tutorial approach. *Insight Non-Destructive Testing and Condition Monitoring, 45(5),* 344-353.

Lee, K.J., Lee, T.M., Yang, M.Y. (2007). Tool wear monitoring system for CNC end milling using a hybrid approach to cutting force regulation. *International Journal of Advanced Manufacturing Technology, 32,* 8-17.

Li, D., & Mathew, J. (1990). Tool wear and failure monitoring techniques for turning- A review. *International Journal of Machine Tools and Manufacture, 30(4),* 579-598.

Li, L., & An, Q. (2016). An in-depth study of tool wear monitoring technique based on image segmentation and texture analysis. *Measurement, 79,* 44-52.

Li, X. (2002). A brief review: Acoustic emission method for tool wear monitoring during turning. *International Journal of Machine Tools and Manufacture, 42(2),* 157-165.

Li, X. (2005). Development of current sensor for cutting force measurement in turning. *IEEE Transactions on Instrumentation and Measurement, 54(1),* 289-296.

Li, X.Q., Wong, Y.S., & Nee, A.Y.C. (1998). Comprehensive identification of tool failure and chatter using a parallel multi-ART2 neural network. *Journal of Manufacturing Science and Engineering, 120(2),* 433-442.

Liao, Y., & Stephenson, D.A. (2010). A multifeature approach to tool wear estimation using 3D workpiece surface texture parameters. *Journal of Manufacturing Science and Engineering, 132(6),* 1-7.

Liao, Z., Gao, D., Lu, Y., & Lv, Z. (2016). Multi-scale hybrid HMM for tool wear condition monitoring. *International Journal of Advanced Manufacturing Technology, 84(9),* 2437-2448.

Lima, J.G., Avila, R.F., Abrao, A.M., Faustino, M., & Davim, J.P. (2005). Hard turning: AISI 4340 high strength low alloy steel and AISI D2 cold work tool steel. *Journal of Materials Processing Technology, 169(3),* 388-395.

Lin, W.S. (2008). Modeling the surface roughness for fine turning of AISI stainless steel. *Key Engineering Materials, 364-366,* 644-648.

Liu, T.I., Song, S.D., Liu, G., & Wu, Z. (2013a). Online monitoring and measurements of tool wear for precision turning of stainless steel parts. *International Journal of Advanced Manufacturing Technology, 65(9),* 1397-1407.

Liu, C., Wu, J., Li, G., & Tan, G. (2013b). Frequency-spectrum characteristics of force in end milling with tool wear and eccentricity. *International Journal of Advanced Manufacturing and Technology, 67(1),* 925-938.

Maia, L.H.A., Abrao, A.M., Vasconcelos, W.L., Sales, W.F., & Machado, A.R. (2015). A new approach for detection of wear mechanism and determination of tool life in turning using acoustic emission. *Tribology International, 92,* 519-532.

Manda, S. (2014). Applicability of tool condition monitoring methods used for conventional milling in micromillig: A comparative review. *Journal of Industrial Engineering, 2014,* 1-8.

Mallat, S.G. (1989). A theory of multiresolution signal decomposition: the wavelet representation. *IEEE Transactions on Pattern and Machine Intelligence, 11(7),* 674-693.

Marinescu, I., & Axinte, D. (2008). A critical analysis of effectiveness of acoustic emission signal to detect tool and workpiece malfunction in milling operations. *International Journal of Machine Tools and Manufacture, 48(10),* 1148-1160.

Marinescu, I., & Axinte, D. (2009). A time-frequency acoustic emission-based monitoring technique to identify workpiece surface malfunction in milling with multiple teeth cutting simultaneously. *International Journal of Machine Tools and Manufacture, 49(1),* 53-65.

Mazzeo, A.D., Stein, A.J., Trumper, D.L., & Hocken, R.J. (2009). Atomic force microscope for accurate dimensional metrology. *Precision Engineering, 33(2),* 135-149.

Meddour, I., Yallese, M.A., Khattabi, R., Elbah, M., & Boulanouar, L. (2015). Investigation and modeling of cutting forces and surface roughness when hard turning of AISI 52100 steel with mixed ceramic tool: cutting conditions optimization. *International Journal of Advanced Manufacturing Technology, 77(5),* 1387-1399.

Mook, W.K., Shahabi, H.H., & Ratnam, M.M. (2009). Measurement of nose radius wear in turning tools from a single 2D image using machine vision. International *Journal of Advanced Manufacturing Technology, 43(3),* 217-225.

Nabil, B.F., & Mabrouk, M. (2006). Effects of random aspects of cutting tool wear on surface roughness and tool life. *Journal of Materials Engineering and Performance, 15(5),* 519-524.

Nakao, Y., & Dornfeld, D.A. (2003). Diamond turning using position and AE dual feedback control system. *Precision Engineering, 27(2),* 117-124.

Neslušan, M., Mičieta, B., Mičietová, A., Čilliková, M., & Mrkvica, I. (2015). Detection of tool breakage during hard turning through acoustic emission at low removal rates. *Measurement, 70,*1-13.

Oraby, S.E., & Alaskari, A.M. (2008). Surface topography assessment techniques based on an in-process monitoring approach of tool wear and cutting force signature. *Journal of Brazilian Society of Mechanical Sciences and Engineering, 30(3),* 221-230.

Oraby, S.E., Al-Modhuf, A.F., & Hayhurst, D.R. (2005). A diagnostic approach for turning tool based on the dynamic force signals. *Journal of Manufacturing Science and Engineering, 127(3),* 463-475.

O'Sullivan, D., & Cotterell, M. (2001). Temperature measurement in single point turning. *Journal Material Processing Technology, 118(1-3),* 301-308.

Otsu, N. (1979). A Threshold Selection Method from Gray-Level Histogram. *IEEE Transactions on Systems, Man and Cybernetics, 9(1),* 62-66.

Özel, T. & Davim, J.P. (2009). *Intelligent Machining*. London, UK: Wiley.

Özel, T., Karpat, Y., Figgueria, L., & Davim, J.P. (2007). Modelling of surface finish and tool flank wear in turning of AISI D2 steel with ceramic wiper inserts. *Journal of Materials Processing Technology, 189(1-3),*192–198.

Özel, T., Tsu-Kong, H., & Zeren, E. (2005). Effect of cutting edge geometry, workpiece hardness, fed rate and cutting speed on surface roughness and forces in finish turning of hardened AISI H13 steel. *International Journal of Advanced Manufacturing Technology, 25(3),* 262–269.

Pampu, N.C. (2011). Study the effect of the short time Fourier transform configuration on EEG spectral estimates. *Electronics and Telecommunications, 52(4),* 26-29.

Patil, S.P., & Tilekar, D.M. (2014). Tool wear detection of cutting tool using Matlab software. *International Journal of Engineering and Technical Research, 2 (11),* 362-366.

Pavel, R., Marinescu, J., Dei, M., & Pillar, J. (2005). Effect of tool wear on surface finish for a case of continuous and interrupted hard turning. *Journal of Materials Processing Technology, 170(1-2),* 341-349.

Penedo, F., Haber, R.E., Gajate, A., & Toro, R.M. (2012). Hybrid incremental modeling based on least square and fuzzy NN for monitoring tool wear in turning processes. *IEEE Transactions on Industrial Informatics, 8(4),* 964-973.

Penalva, M.L., Arizmendi, M., Diaz, F., & Fernandez, J. (2002). Effect of tool war on roughness in hard turning. *CIRP Annals-Manufacturing Technology, 51(1),* 57-60.

Pfeifer, T., & Wiegers, L. (2000). Reliable tool wear monitoring by optimized image and illumination control in machine vision. *Measurement, 28(3),* 209-218.

Rad, J.S., Zhang, Y., Aghazadeh, F., & Chen Z.C. (2014). *A study on tool wear monitoring using time-frequency transformation techniques.* Paper presented at International Conference on Innovative Design and Manufacturing, Montreal, Quebec, Canada.

Rafiee, J., & Tse, P.W. (2009). Use of autocorrelation of wavelet coefficients for fault diagnosis. *Mechanical Systems and Signal Processing, 23(5),* 1554-1572.

Rehorn, A.G., Jiang, J., & Orban, P.E. (2005). State-of-the-art methods and results in tool condition monitoring: a review. *International Journal of Advanced Manufacturing Technology, 26(7),* 693–710.

Ren, Q., Balazinski, M., Baron, L., & Jemielniak, K. (2011). TSK fuzzy modeling for tool wear condition in turning processes: An experimental study. *Engineering Applications of Artificial Intelligence, 24(2),* 260-265.

Roy, S., Bhattacharyya, A., & Banerjee, S. (2007). Analysis of effect of voltage on surface texture in electrochemical grinding by autocorrelation function. *Tribology International, 40(9),* 1387-1393.

Runola, J.P., Moon, K.S., & Sutherland, J.W. (1994). The effects of tool wear on the wavelength structure of a turned surface profile. *Transactions of NAMRI/SME, 22,* 105-109

Salgado, D.R., & Alonso, F.J. (2007). An approach based on current and sound signals for in-process tool wear monitoring. *International Journal Machine Tools and Manufacture, 47(14),* 2140-2152.

Samraj, A., Sayeed, S., Raja, J.E., Hossen, J., & Rahman, A. (2011). Dynamic clustering estimation of tool flank wear in turning process using SVD models of the emitted sound signals. *World Academy Science Engineering Technology, 56,* 1151-1155.

Sandvik Coromant Catalogue, 2015. Available in: http://www.sandvik.coromant.com

Sanjanwala, A., Choudhury, S.K., & Jain, V.K. (1990). Online tool wear sensing and compensation during turning. *Precision Engineering, 12(2),* 81-84.

Sata, T., Li, M., Takata, S., Hiraoka, H., Li, C.Q., Xing, X.Z., & Xiao, X.G. (1985) Analysis of surface roughness generation in turning operation and its application. *Annals of CIRP, 34(1),* 473-476.

Shahabi, H.H., & Ratnam, M.M. (2009a). In-cycle monitoring of tool nose wear and surface roughness of turned parts using machine vision. *International Journal of Advanced Manufacturing Technology, 40(11)*, 1148-1157.

Shahabi, H.H., & Ratnam, M.M. (2009b). Assessment of flank wear and nose radius wear from workpience roughness profile in turning operation using machine vision. *International Journal of Advanced Manufacturing Technology, 43(1)*, 11-21.

Sharma, V.S., Sharma, S.K., & Sharma, A.K. (2008) Cutting tool wear estimation for turning. *Journal of Intelligent Manufacturing*, 19(1), 99-108

Shi, D.F., & Gindy, N.N. (2007). Development of an online machining process monitoring system: Application in hard turning. *Sensors and Actuators A, 135(2),* 405-414.

Sick, B. (2002). Online and indirect tool wear monitoring in turning using artificial neural networks: a review of more than a decade of research. *Mechanical Systems and Signal Processing*, *16(4),* 487-546.

Siddhpura, A., & Paurobally, R. (2013). A review of flank wear prediction methods for tool condition monitoring in a turning process. *International Journal of Advanced Manufacturing Technology, 65(1),* 371-393.

Sikdar, S.K., & Chen, M. (2002). Relationship between tool flank wear area and component forces in single point turning. *Journal of Materials Processing Technology, 128(1-3),* 210-215.

Silva, R.G., Reuben, R.L., Baker, K.J., & Wilcox, S.J. (1998). Tool wear monitoring of turning operations by neural network and expert system classification of a feature set generated from multiple sensors. *Mechanical Systems and Signal Processing, 12(2),* 319-332.

Sivasakthivel, P.S., & Sudhakaran, R. (2013). Optimization of machining parameters on temperature rise in end milling of Al 6063 using response surface methodology and genetic algorithm. *International Journal of Advanced Manufacturing and Technology, 67(9),*2313-2323.

Sobiyi, K., Sigalas, I., Akdogan, G., & Turan, Y. (2015). Performance of mixed ceramics and CBN tools during hard turning of martensitic stainless steel. *International Journal of Advanced Manufacturing and Technology, 77(5),* 861-871.

Sortino, M. (2003). Application of statistical filtering for optical detection of tool wear. *International Journal of Machine Tools and Manufacture, 43(5),* 493-497.

Tabatabai, A.J., & Mitchell, R. (1984). Edge location to sub-pixel values in digital imagery. *IEEE Transactions on Pattern Analysis and Machine Intelligence, 6(2),* 188-201.

Tekiner, Z., & Yesilyurt, S. (2004). Investigation of the cutting parameters depending on process sound during turning of AISI 304 austenitic stainless steel. *Materials and Design, 25(6),* 507-513.

Teti, R., Jemielniak, K., O'Donnell, G., & Dornfeld, D. (2010). Advanced monitoring of machining operations. *CIRP Annals-Manufacturing Technology, 59(2),* 717-739.

Thomas, M., Beauchamp, Y., Youssef, A.Y., & Masounave, J. (1996). Effect of tool vibrations on surface roughness during lathe dry turning process. *Computers and Industrial Engineering, 31(3/4),* 637-644.

Tsao, C.C. (2002). Prediction of flank wear of different coated drills for JIS SUS 304 stainless steel using neural network. *Journal of Materials Processing Technology, 123(3),* 354-360.

Wang, H.L., Shao, H., Chen, M., & Hu, D.J. (2003). Online tool breakage monitoring in turning. *Journal of Materials Processing Technology, 139(1-3),* 237-242.

Wang, L.H., & Gao, R.X. (2006). *Condition Monitoring and Control for Intelligent Manufacturing.* Germany: Springer.

Wang, W.H., Hong, G.S. & Wong, Y.S. (2006). Flank wear measurement by a threshold independent method with sub-pixel accuracy. *International Journal of Machine Tools and Manufacture, 46(2),* 199-207.

Wheeler, A.J., & Ganji, A.R. (2010). *Introduction to Engineering Experimentation*. New Jersey: Pearson Education.

Yesilyurt, I. (2006). End mill breakage detection using mean frequency analysis of scalogram. *International Journal of Machine Tool and Manufacture, 46(3-4),* 450-458.

Yin, Z., Huang, C., Yuan, J., Zou, B., Liu, H., & Zhu, H. (2015). Cutting performance and life prediction of an Al_2O_3 /TiC micro-nano-composite ceramic tool when machining austenitic stainless steel. *Ceramics International, 41(5),* 7059-7065.

Youn, J.W., Yang, M.Y., & Park, H.Y. (1994). Detection of cutting tool fracture by dual signal measurements. *International Journal Machine Tools and Manufacture*, *34(4),* 507-525.

Zhang, J., Zhang, C., Guo, S., & Zhou, L. (2012). Research on tool wear detection based on machine vision in end milling process. *Production Engineering, 6(4),* 431-437.

Zhang, K.F., Yuan, H.Q., & Nie, P. (2015). A method for tool condition monitoring based on sensor fusion. *Journal of Intelligent Manufacturing, 26(5),*1011–1026.

Zhou, J.M., Andersson, A., & Stahl, J.E. (2003). The monitoring of flank wear on the CBN tool in the hard turning process. *International Journal of Advanced Manufacturing Technology, 22(9),* 697-702.

Zhu, K., Wong, Y.S., & Hong, G.S. (2009). Wavelet analysis of sensor signals for tool condition monitoring: A review and some new results. *International Journal of Machine Tools and Manufacture, 49(7-8),* 537-553.

Zubaydi, A., Haddara, M.R., & Swamidas, A.S.J. (2000). On the use of autocorrelation function to identify the damage in the side shell of a ship's hull. *Marine Structures*, *13*, 537-551.